arXiv:1205.6319v1 [astro-ph.CO] 29 May 2012

Uncertainties in SDSS galaxy parameter determination: 3D photometrical modelling of test galaxies and restoration of their structural parameters

Elmo Tempel[a,b,*], Antti Tamm[a], Rain Kipper[a,c], Peeter Tenjes[a,c]

[a] *Tartu Observatory, Observatooriumi 1, 61602 Tõravere, Estonia*
[b] *National Institute of Chemical Physics and Biophysics, 10143 Tallinn, Estonia*
[c] *Institute of Physics, Tartu University, Tähe 4, 51010 Tartu, Estonia*

Abstract

Is it realistic to recover the 3D structure of galaxies from their images? To answer this question, we generate a sample of idealised model galaxies consisting of a disc-like component and a spheroidal component (bulge) with varying luminosities, inclination angles and structural parameters, and component density following the Einasto distribution. We simulate these galaxies as if observed in the SDSS project through *ugriz* filters, thus gaining a set of images of galaxies with known intrinsic properties. We remodel the galaxies with a 3D galaxy modelling procedure and compare the restored parameters to the initial ones in order to determine the uncertainties of the models.

Down to the r-band limiting magnitude 18, errors of the restored integral luminosities and colour indices remain within 0.05 mag and errors of the luminosities of individual components within 0.2 mag. Accuracy of the restored bulge-to-disc ratios (B/D) is within 40% in most cases, and becomes even worse for galaxies with low B/D due to difficulties in reconstructing their bulge properties. Nevertheless, the general balance between bulges and discs is not shifted systematically. Inclination angle estimates are better for disc-dominated galaxies, with the errors remaining below 5° for galaxies with $\mathrm{B/D} < 2$. Errors of the recovered sizes of the galactic components are less than 10% in most cases. Axial ratios and the parameter N of Einasto's distribution (similar to the Sérsic index) are relatively inaccurate, but can provide statistical estimates for large samples. In general, models of disc components are more accurate than models of bulge components for geometrical reasons.

Keywords: methods: numerical; galaxies: bulges; galaxies: photometry; galaxies: structure

1. Introduction

In studies of galactic structures, galactic parameters are usually derived by analysing 1-dimensional or 2-dimensional surface brightness distributions measured from the images. In the former case, the surface brightness profile along the major axis (or an arbitrary line) of the galaxy, either measured directly or obtained by averaging along elliptical contours, is approximated with some model distributions, while in the latter case, the whole galaxy image is approximated with a model distribution, e.g. with the automated fitting tools GALFIT (Peng et al., 2010), GIM2d (Simard et al., 2002), or BUDDA (de Souza et al., 2004).

In reality, galaxies are 3-dimensional objects, thus a physically more justified approach would be fitting of a 3-dimensional model to the observations. In this case, for example, inevitable degeneracies between various parameters (e.g. the inclination an-

---

[*] Corresponding author at: Tartu Observatory, Observatooriumi 1, 61602 Tõravere, Estonia

Email addresses: `elmo@aai.ee` (Elmo Tempel), `atamm@aai.ee` (Antti Tamm), `rain@aai.ee` (Rain Kipper), `peeter.tenjes@ut.ee` (Peeter Tenjes)

gle and the thickness of a galactic component) are more easily disentangled. By constraining the models with just a few assumptions about the geometry of the galactic components, one should be able to reduce such uncertainties significantly. Furthermore, a 3-dimensional model directly yields distribution of the gravitational potential of the galaxy for comparison with kinematical data and simplifies estimating the intrinsic dust effects along any given line of sight.

A 3-dimensional galaxy modelling procedure has to be tested thoroughly prior to applying to the observational data in order to clarify the reliability and uniqueness of the determined galactic parameters. Most importantly, it is needed to know how the parameter uncertainties depend on the apparent magnitude, size, compactness, shape, inclination and other general properties of the galaxy, and whether the particular approach is causing any systematic errors. The limitations of the model should be tested in a realistic situation of actual telescopic data with all the involved observational uncertainties included.

In the present paper we describe the construction and usage of a 3-dimensional galaxy model which can be fitted to single or multi-wavelength galaxy imaging. We create a sample of simple idealistic 2-component (bulge + disc) test galaxies. Although we acknowledge the recent findings about fundamental differences between the origin of disc galaxy bulges and elliptical galaxies, we make no such distinction here, since we are interested in the structural properties only and not the actual nature of the components. We plant these galaxies into artificial Sloan Digital Sky Survey (SDSS) images and remodel them using our 3-dimension modelling software. By comparing the restored galactic parameters to the initial ones, we determine the limitations of the interplay between SDSS imaging and our modelling software. Above all, we are interested in the reliability of the recovered inclination angles and axial ratios of galactic components, since the potential ability to determine these parameters is the main advantage of our model over the 1- and 2-dimensional models.

Our present analysis is based on the SDSS Data Release 8 (Aihara et al., 2011). We have used the main galaxy sample, downloaded from the Catalog Archive Server (CAS). We have limited the galaxy sample to be brighter than the *r*-band Petrosian magnitude 17.77. The details of the used sample are described in Tempel and Tago (2012). The DR 8 sample is greatly improved over the previous data releases, in the sense that all the imaging data have been reprocessed with an improved sky-subtraction algorithm and a final, self-consistent photometric recalibration and flat-field determination. This improvement makes the DR 8 a good testing ground for detailed photometrical modelling.

2. A sample of modelled SDSS galaxies

To be able to give a correct estimate of the precision of a galaxy modelling technique, one needs a sufficiently large sample of test objects, for which the actual properties are well known. One would probably find that the best way to know the properties of a galaxy is to construct the galaxy oneself.

We have constructed a sample of 1000 test galaxies on the basis of actual objects from the SDSS, covering a maximally broad range of the main properties: luminosities, luminosity distributions, sizes, axial ratios, bulge-to-disc ratios and inclination angles. Considering forthcoming applications of the model, galaxies with *r*-filter luminosities higher than 17.77 mag were selected from the original SDSS images, which is the completeness limit of the spectroscopic sample of the SDSS (Strauss et al., 2002).

The atlas (prefix ‘fpAtlas’), mask (prefix ‘fM’), and point-spread-function (prefix ‘psField’) images of the observed galaxies were retrieved from the SDSS Data Archive Server (DAS). We used the SDSS software utilities `readAtlasImages` and `readPSF` for the atlas and PSF images, respectively. Masks were applied to the atlas images, using galaxy positions (given by `rowc` and `colc` in SDSS CAS). The model objects were created from the actual galaxy images using the same technique as described in Sect. 3.1. In this step, the accuracy of the model is not crucial, since we would use only the modelled parameters further on. As a result we obtained 1000 idealised bulge-disc objects with a wide range of parameters.

Next we simulated these ideal model galaxies as if observed by the SDSS. The surface brightness distributions in *ugriz* colours of the test galaxies were convolved with the SDSS point spread function (PSF). Poisson noise was added to every pixel according to

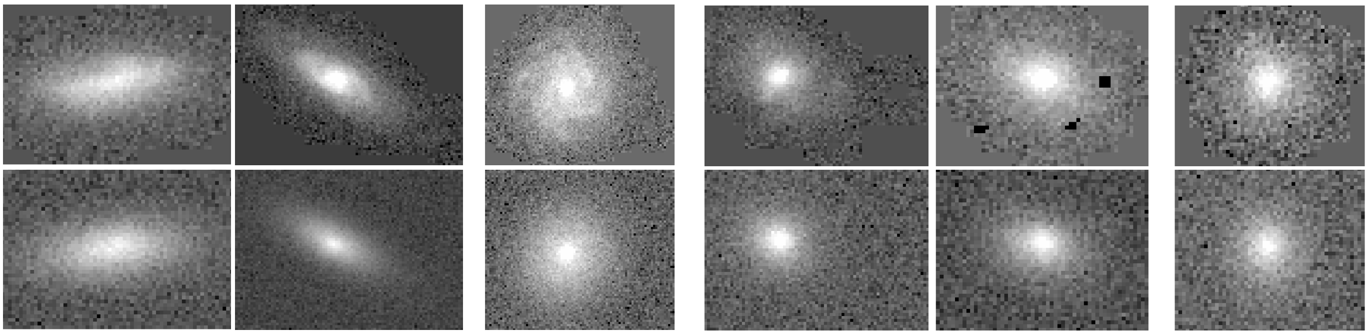

Figure 1: Examples of the original (*upper row*) and simulated (*lower row*) SDSS images of the objects in our test galaxy sample. In the simulated images, the SDSS PSF and noise have been applied to the model galaxies (see text for more information). The smoothed and black areas in the original images are masked pixels.

the intensity value of the pixel. Observational noise (the sum of sky foreground and background and the instrumental noise) was taken from regions with no detectable objects in the actual SDSS observational frames.

After these steps we possessed the "SDSS images" of the 1000 test-galaxies with known intrinsic parameters. Some typical representatives of these simulated images are shown in the lower row of Fig. 1. For visual comparison, the images of the corresponding real SDSS galaxies are given in the upper row of the same figure. While the actual intrinsic parameters of the upper row objects are unknown, the structure of the lower row objects is known precisely.

For the subsequent analysis, we have used only the simulated test sample of galaxies with known parameters. Besides, we have also conducted some illustrative tests on the real SDSS sample as described in Sect. 5.

3. Description of the three-dimensional photometrical model

3.1. General description of the photometrical model

We use a sufficiently flexible model for describing the spatial distribution of the luminosity of a galaxy. The model galaxy is given as a superposition of its individual stellar components. Each component is approximated by an ellipsoid of rotational symmetry with a constant axial ratio q; its spatial density distribution follows Einasto's law

$$l(a) = l(0) \exp\left[-\left(\frac{a}{ka_0}\right)^{1/N}\right], \qquad (1)$$

where $l(0) = hL/(4\pi q a_0^3)$ is the central density and L is the luminosity of the component; $a = \sqrt{r^2 + z^2/q^2}$, where r and z are two cylindrical coordinates. We make use of the harmonic mean radius a_0 as a good characteriser of the real extent of the component. The coefficients h and k are normalising parameters, dependent on the structure parameter N (see appendix B of Tenjes et al., 1994). The luminosity density distribution (Eq. 1) proposed by Einasto (1965) is similar to the Sérsic law (Sérsic, 1968) for surface densities (Tamm and Tenjes, 2006).

The density distributions of all visible components are projected along the line of sight and their sum yields the surface brightness distribution of the model

$$L(A) = 2 \sum_j \frac{q_j}{Q_j} \int_A^{\infty} \frac{l_j(a) a \, \mathrm{d}a}{(a^2 - A^2)^{1/2}}, \qquad (2)$$

where A is the major semi-axis of the equidensity ellipse of the projected light distribution and Q_j are their apparent axial ratios $Q^2 = \cos^2 i + q^2 \sin^2 i$. The inclination angle between the plane of the galaxy and the plane of the sky is denoted by i. The summation index j designates each visible component.

Equation (2) gives the surface brightness of the galaxy for a given line of sight. In principle, this simple model can be further specified, by adding ring-like structures (see, e.g. Einasto et al., 1980) and taking account the interstellar dust inside the galaxy (see, e.g. Tempel et al., 2010, 2011). These details are ignored in the present analysis, since the SDSS dataset alone is not detailed enough for the inclusion of such components with sufficient confidence.

3.2. *Bulge + disc model for SDSS galaxies*

Our sample of SDSS galaxies includes both early and late type galaxies. We apply simple bulge + disc models to all galaxies independently of their morphological type. Galaxies are fitted with two Einasto's profiles (Eq. 1); the structural parameters a_0, q and N for the bulge and the disc are independent of each other as well as the component luminosities in *ugriz* filters.

The initial guess for the centre and position angle parameters is taken from the SDSS CAS, where each galaxy has been approximated by simple bulge and disc models. During the modelling procedure, these parameters are adjusted separately for each filter. The same centre coordinates, position angle and inclination is assumed for the bulge and the disc of each galaxy.

In order to keep the components realistic, we have fixed some parameter limits during modelling. For the bulges, we have set the lower limit of N 2.0 to exclude disc-like profiles and the upper limit at $N = 6.0$ to avoid unrealistically compact cores. For the discs, we have set $N = 2.5$ as the upper limit. For the axial ratio q, we have set the lower limit at 0.4 for the bulges and the upper limit at 0.3 for the discs.

3.3. *Modelling procedure*

We have used all the five SDSS filters (*ugriz*) in our modelling procedure. However, only the *gri* filters were used for determining the structural parameters since the uncertainties for *u* and *z* imaging are the largest. The *u* and *z* observations were then used for calculating the bulge and disc luminosities for these filters according to the structural model.

Correctness of the model fit was estimated by using the χ^2 value, defined by

$$\chi^2 = \frac{1}{N_{\mathrm{dof}}} \sum_{\nu} \sum_{x,y \in \mathrm{mask}} \frac{(f^{\nu}_{\mathrm{obs}}(x,y) - f^{\nu}_{\mathrm{model}}(x,y))^2}{\sigma^{\nu}(x,y)^2}, \quad (3)$$

where N_{dof} is the number of degrees of freedom in the fit; $f^{\nu}_{\mathrm{obs}}(x,y)$ and $f^{\nu}_{\mathrm{model}}(x,y)$ are the observed and modelled fluxes at the given pixel (x,y) and index ν indicates the filter (*ugriz*); $\sigma(x,y)$ is the Poisson error at each pixel. The summation is taken over all filters (ν) and all pixels of each galaxy as defined by the corresponding mask. In the present study the number of free parameters is 16: the structural parameters a_0, q, N and the *gri* luminosities for each component and the central coordinates, inclination angle and the position angle of the galaxy. Note that Eq. 3 gives an equal weight to each collected photon regardless of its place of birth in the galaxy.

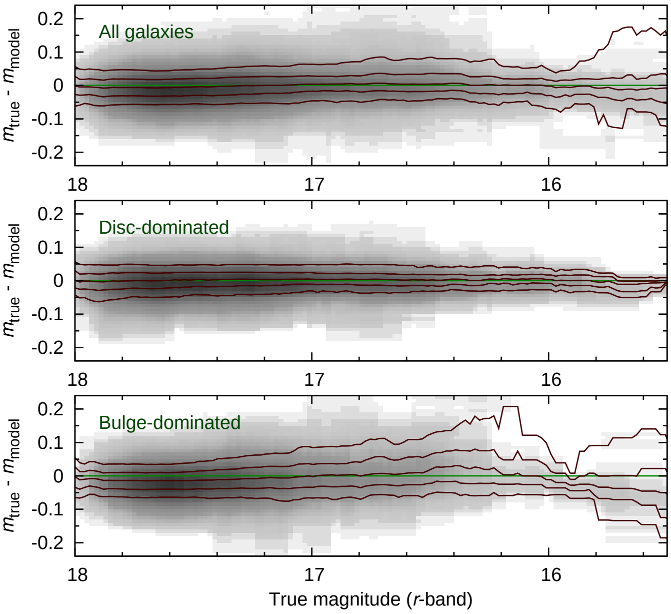

Figure 2: Distribution of differences between the true and restored integral luminosities of all (*upper panel*), disc-dominated (*middle panel*), and bulge-dominated (*lower panel*) galaxies, as a function of galaxy luminosity. Intensity of the *shaded regions* expresses the number of objects corresponding to each distribution bin. *Red solid lines* show the 0.1, 0.25, 0.5, 0.75, and 0.9 quantiles of the distribution.

To minimise the χ^2 we have used the downhill simplex method of Nelder and Mead from the Numerical Recipe library. This method is quite simple and efficient in searching large parameter spaces. We have also tried other non-linear least-square fitting algorithms (e.g. Levenberg-Marquardt algorithm), but the simulated annealing method by Nelder and Mead was the fastest one when the initial parameters where sufficiently close to the real parameters. In the present case, since the initial parameters were taken from the original SDSS fits, such a requirement was fulfilled.

4. Results and discussion

To test the restoration accuracy of the intrinsic properties of galaxies, we have calculated differences

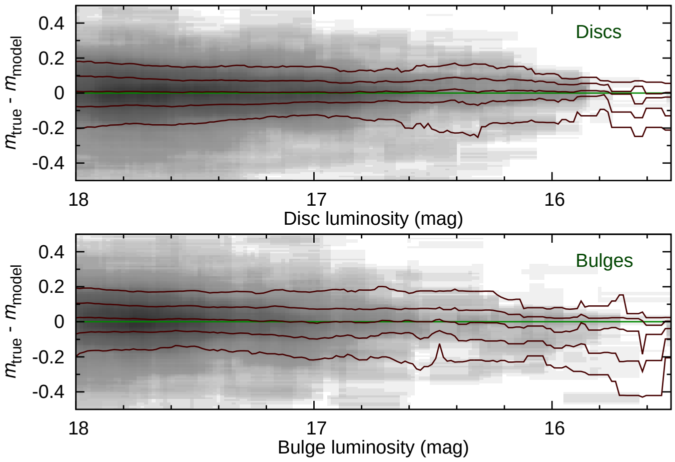

Figure 3: Distribution of differences between the true and restored integral luminosities of the disc (*upper panel*) and bulge (*lower panel*) components of the galaxies as a function of the component luminosity. *Red solid lines* show the 0.1, 0.25, 0.5, 0.75, and 0.9 quantiles of the distribution.

between the parameters of the original test sample galaxies and the modelled ones. The restoration accuracy is analysed for whole galaxies as well as separately for bulge and disc components. Distinction is made also between disc-dominated and bulge-dominated galaxies on the basis of the bulge-to-disc luminosity ratio of the original galaxies in the r filter: galaxies with the ratio less than 0.7 are taken to be disc dominated and galaxies with the ratio larger than 1.3 are taken to be bulge dominated.

4.1. *Restoring the intrinsic luminosities and colours*

Differences between the original and restored integral r-band luminosities of the galaxies are shown in Fig. 2; the qualitative results for the other SDSS filters are similar. As indicated by the quantile lines in the figure, differences are below 0.05 mag for most of the galaxies, almost independently of galaxy luminosity. The errors are similar to the original SDSS galaxy catalogue errors of the total luminosities of galaxies, thus indicating the dominance of the photometric uncertainties of the images over the accuracy of the modelling or measuring technique. For brighter bulge-dominated galaxies, the errors become slightly larger. Luminosities are systematically slightly underestimated, probably related to the uncertainties of other parameters of these galaxies.

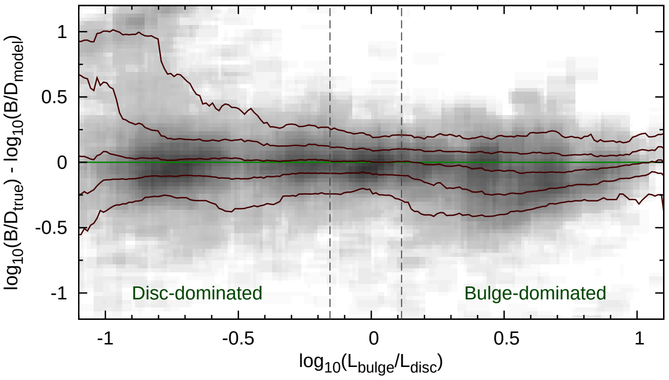

Figure 4: Distribution of differences between the true and restored bulge-to-disc ratios as a function of bulge-to-disc ratio. *Red solid lines* show the 0.1, 0.25, 0.5, 0.75, and 0.9 quantiles of the distribution. Vertical *dashed lines* separate the regions of disc-dominated and bulge-dominated galaxies as defined in this study. For galaxies with bulge-to-disc ratio less than 0.2, bulge component is poorly determined, yielding large uncertainties. On an average, no general systematic shift of the components fraction is introduced.

Figure 3 shows differences between the true and modelled integral luminosities for disc and bulge components of galaxies. In general, the differences are somewhat larger (within 0.2 mag) than for the whole galaxies, which is a natural result of the degeneracy between bulge and disc components. In most cases, the bulge and disc luminosity determination errors compensate each other and the total luminosity is conserved. For bright bulges, an increasing luminosity underestimation can be noted, probably for similar reasons as in the case of bright bulge-dominated galaxies.

Figure 4 shows differences between the modelled and true bulge-to-disc ratios (B/D) as a function of true B/D. It is seen that for B/D $>$ 0.3, the errors are independent of the initial B/D and typically stay within ±40%. For galaxies with very small B/D (close to 0.2), the bulge component is rather inaccurately recovered, yielding large uncertainties in B/D determination. However, the total luminosity of the galaxy remains almost unaffected. On the other hand, the disc luminosity is estimated accurately also in the case of high B/D. Despite the generally low accuracy of the restored B/D, it is important to note that on an average, no systematic shift of the balance between bulges and discs is artificially introduced.

The relative and absolute differences between the true and modelled luminosities of galaxies as a function of distance from galaxy centre are presented in

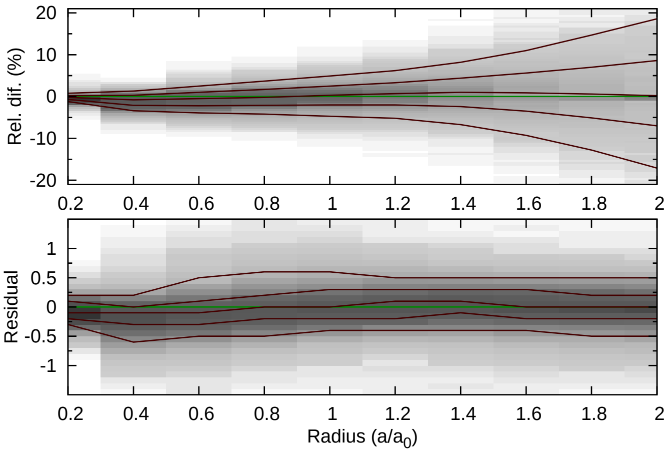

Figure 5: Luminosity difference distribution of true and modelled galaxies, as measured within thin concentric rings as a function of ring radius. *Upper panel:* luminosity differences divided by the luminosity (per cent). *Lower panel:* residual values in the SDSS standard units, nanomaggies. Ring radii are presented as a fraction of the harmonic mean radius of the given galaxy. *Red solid lines* show the 0.1, 0.25, 0.5, 0.75, and 0.9 quantiles of the distribution.

Fig. 5. The luminosities are measured within thin concentric rings. The ring radii are presented as fractions of the harmonic mean radii a_0 of the galaxies (more precisely, as fractions of the radii of the larger component of the given galaxy). For inner regions, the modelling accuracy stays well within the 5% limits. As the surface brightness drops and noise starts to dominate in the outer regions, the models become less accurate as expected, but no systematic trend is introduced. The lower panel in Fig. 5 shows the residuals measured from the simulated SDSS images inside concentric circles after the subtraction of the model. The residuals are radius-independent, because during our model fitting procedure, the inner and outer luminosities are considered with equal weight (see Sect. 3.3).

Differences between the original and modelled $g - r$ colour indices are presented in Fig. 6. For all the other colour indices, the results are similar. The errors remain within 0.03 mag for most of the galaxies, being smaller than the errors of integral luminosities. This is probably caused by the fact that the fitted model galaxy has the same structural parameters for each filter, thus the errors in the structure recovery are also similar for each filter, leading to quantitatively similar misestimation of the luminosity in each filter and a correspondingly smaller spread in the colour indices. As expected, colours are estimated more accurately for brighter galaxies and galactic components. At the faint end of the sample, the errors increase up to 0.1 mag. Similarly to integral luminosities, colours of disc components are recovered with higher precision than colours of bulge components.

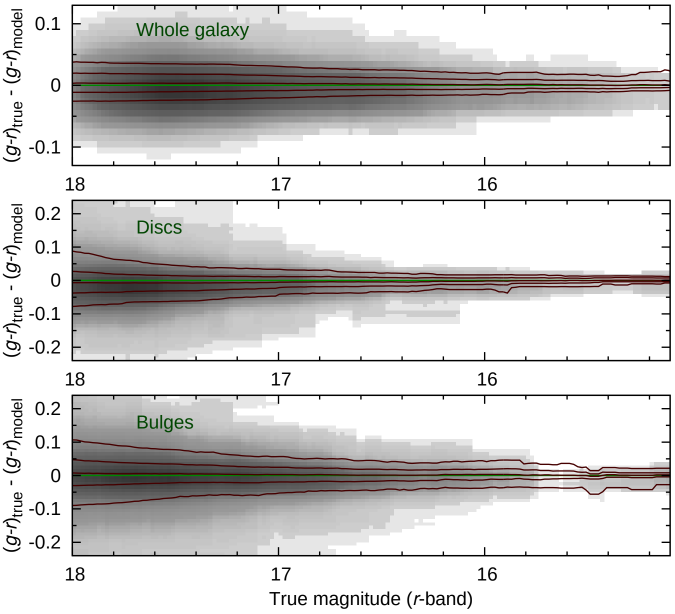

Figure 6: Distribution of differences between true and modelled integral $g - r$ colours for whole galaxies (*upper panel*), for disc components (*middle panel*), and for bulge components (*lower panel*) as a function of luminosity. *Red solid lines* show the 0.1, 0.25, 0.5, 0.75, and 0.9 quantiles of the distribution. In general, differences are smaller than for integral luminosities.

4.2. Restoring the inclination angles of galaxies

The main advantage of 3D modelling of galaxies over 2D modelling is the fact that 3D models yield estimates for the inclination angles of galaxies. However, this advantage comes with a considerable sacrifice of computational time, thus the accuracy of inclination angle estimation is crucial in deciding whether or not 3D modelling is worth attempting.

To measure the inclination angle of galaxies, we have run the modelling code with ten different initial guesses for the inclination angle between 0 (face-on galaxies) and 90° (edge-on galaxies). The reason for this is that our model is sensitive to the initial inclination angle and in many cases, the final fitted inclination angle would lie close to the initial guess value.

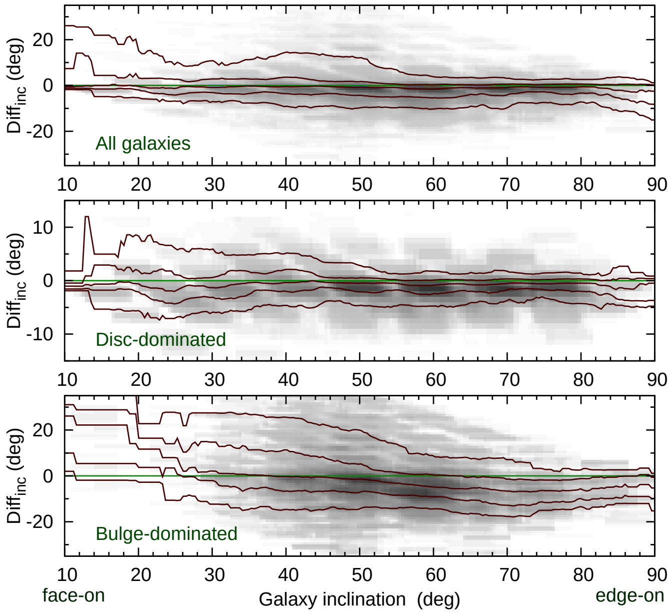

Figure 7: Distribution of differences between the true and restored inclination angles of galaxies for all (*upper panel*), bulge-dominated (*middle panel*), and disc-dominated (*lower panel*) galaxies, presented in degrees. The slight decrease of differences for large inclinations is due the fact that inclination angle cannot be larger than 90°.

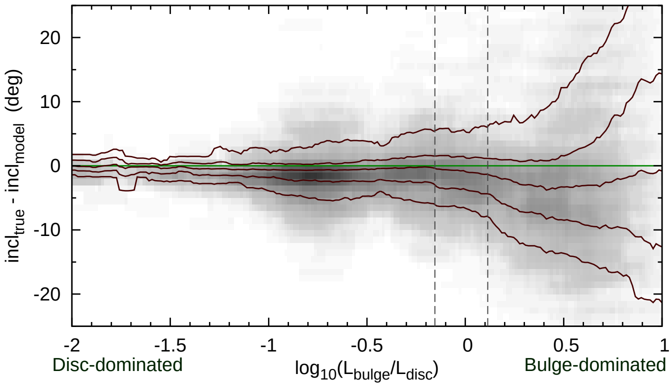

Figure 8: Distribution of differences between the true and restored inclination angles of galaxies as a function of bulge-to-disc ratio. *Vertical dashed lines* separate the regions of disc-dominated and bulge-dominated galaxies as defined in this study. The errors are below 5° for disc-dominated galaxies but worsens while moving toward bulge-dominated (i.e. elliptical) galaxies.

Differences between the true and modelled inclination angles are shown in Fig. 7. For disc-dominated galaxies, the errors are below 5 degrees in most cases, being slightly lower for more edge-on galaxies. The slight decrease of differences for large inclinations is due the fact that inclination angle cannot be larger than 90°. The reader also notices the lack of face-on bulge-dominated galaxies in our sample. Our sample of idealised model galaxies is constructed on the basis on actual objects and the inclination angle is derived assuming axially symmetric galaxies. In reality, bulges and elliptical galaxies are triaxial ellipsoids, yielding no circularly symmetric projections which could be interpreted as a face-on configuration.

Since the inclination angle of a galaxy is related to its disc rather than bulge, the inclination angle restoration accuracy correlates with the bulge-to-disc ratio of the galaxy, as seen in Fig. 8. Differences between the true and restored inclinations start to increase rapidly, when the bulge-to-disc ratio becomes larger than 2–3. Note however that in principal, the inclination angles of real elliptical galaxies cannot be restored (and are difficult to define!) from images since these objects are triaxial ellipsoids.

Based on this test, we can conclude that inclination angles can be restored sufficiently accurately for spiral and S0 galaxies and the additionally required CPU time for 3D modelling is justified, when the inclination angle determination is important.

4.3. *Restoring the structural parameters*

Figure 9 shows relative differences between the true and modelled harmonic mean radius a_0 as a function of component luminosity. The figure shows that for discs, the difference is almost insensitive to the luminosity. Since luminosity correlates with radius, the difference is also insensitive to the disc radius. It is noticeable, that the modelled discs are systematically smaller by about a few per cent. In general, for most of the galaxies, the disc radius is restored with accuracy higher than 10 per cent.

For bulges (lower panel in Fig. 9), the modelled radius a_0 is worser than for discs. For brighter bulges, the modelled radius is five to ten per cent below the true value. This effect is probably responsible for the underestimation of the luminosities of bright bulges.

Figure 10 shows differences between the true and modelled axial ratios q of the galactic components as a function of the radius of the component. Considering the upper limit for the disc axial ratio $q = 0.3$ in the model, the axial ratio accuracy ±0.05 for about half of the test galaxies is satisfactory. For about 20%

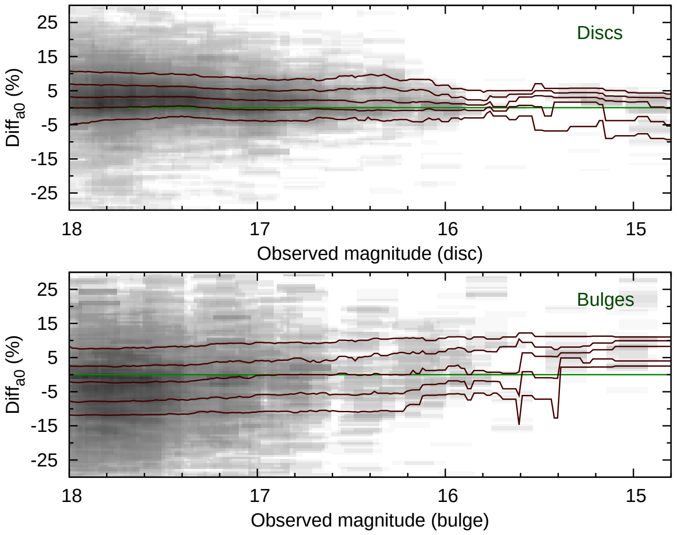

Figure 9: Distribution of differences (per cent) between the original and restored harmonic mean radius a_0 for disc (*upper panel*) and for bulge (*lower panel*) component as a function of the component luminosity. *Red solid lines* show the 0.1, 0.25, 0.5, 0.75, and 0.9 quantiles of the distribution.

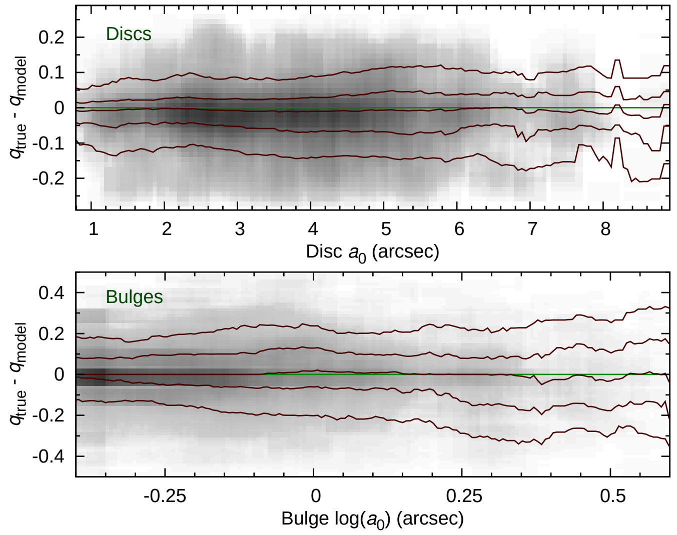

Figure 10: Difference between true and modelled axial ratio q for disc (*upper panel*) and bulge (*lower panel*) components as a function of the component radius a_0. *Red solid lines* show the 0.1, 0.25, 0.5, 0.75, and 0.9 quantiles of the distribution.

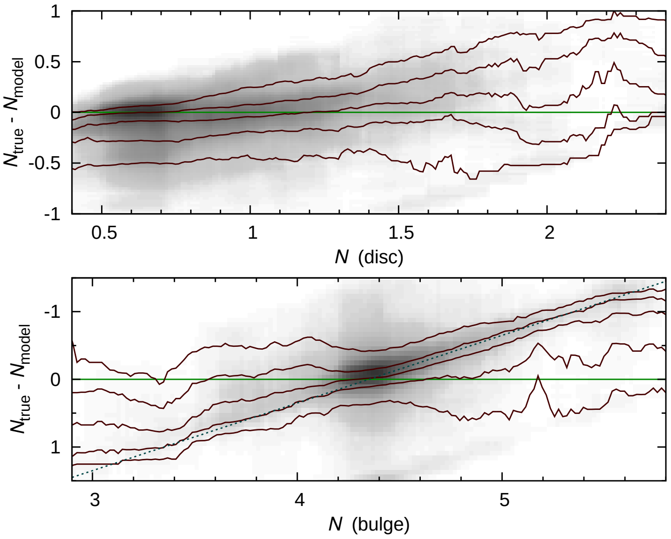

Figure 11: Differences between the true and modelled structural parameter N for disc (*upper panel*) and bulge (*lower panel*) components as a function of N. *Red solid lines* show the 0.1, 0.25, 0.5, 0.75, and 0.9 quantiles of the distribution. The tilt of the distributions is caused by the lower and upper limits for N. The *dotted* straight line in the *lower* panel corresponds to the restored luminosity $N = 4.35$.

of the discs (outside the 0.1 and 0.9 quantile lines), the model estimate totally misses the true value, being off by more than 0.1 (i.e., one third of the allowed range). For the rest, the model accuracy is low, but may provide some statistically reliable results in large surveys. For the bulges, differences seem even larger, but the allowed range for q is also considerably larger (0.4–1.0). Note that similarly the inclination angle, the axial ratio has no clear meaning for real bulges and elliptical galaxies, since these objects are in fact triaxial. Figure 10 also shows that the accuracy of q determination does not depend on the size of the component.

Figure 11 shows differences between the true and modelled values for the structural parameter N. The decreasing trend of both distributions is caused by the lower and upper limits set for N during modelling. Close to these limits, the difference can only be positive or negative, respectively. As expected, the accuracy of N is rather low, staying within about ±0.5 for most of the cases.

For the bulges (lower panel in Fig. 11), we can note clustering around the value $N \approx 4.3$, which corresponds to $N \approx 4$ for the Sérsic distribution (Dhar and Willia 2010). On one hand, this is known to be the most

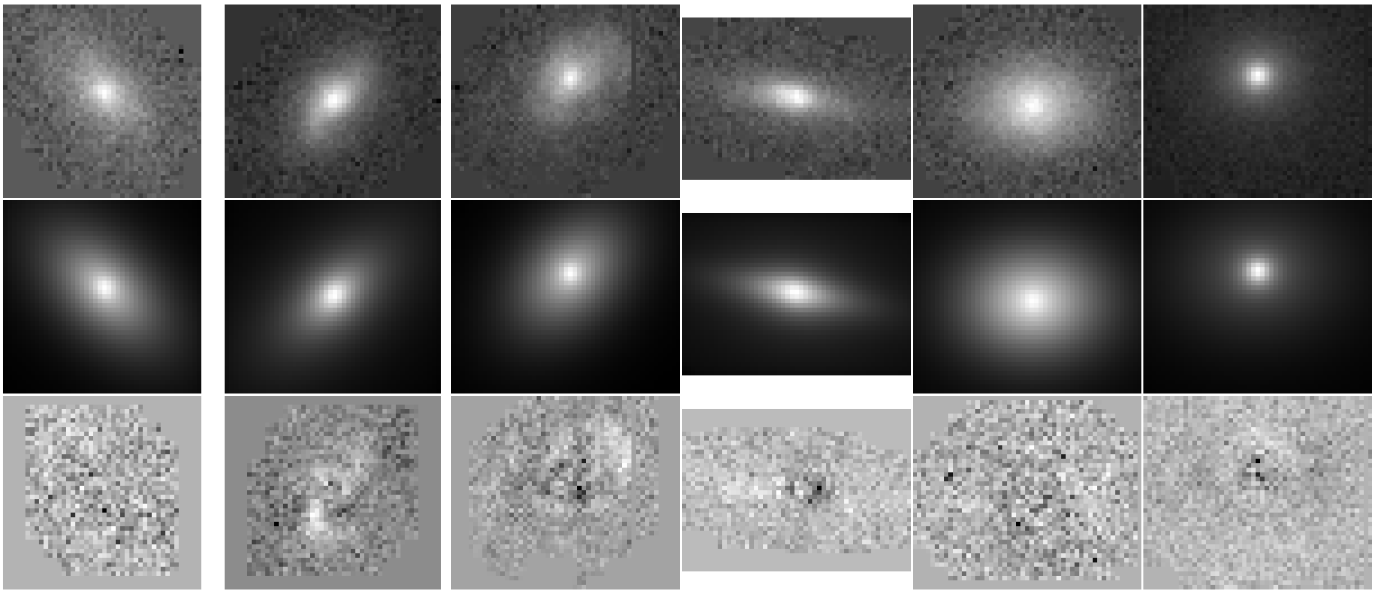

Figure 12: Examples of modelling real SDSS galaxies. *Upper row* shows the original observations, *middle* row shows the PSF-convolved model galaxies, and *lower row* shows the residual images.

typical value for bulges. On the other hand, we have used it as the initial guess value for the bulge components. The dotted line plotted for the restored value $N = 4.35$ indicates that the model has usually found a solution close to the initial value. This suggests that in most cases, it is reasonable to fix the bulge N at 4.3 during modelling and let the parameter free only in the case of the appearance of significant residuals, as has been recently done with 2D models (Simard et al., 2011; Lackner and Gunn, 2012).

5. Modelling the real SDSS images

So far we have only analysed the modelling results of idealistic test galaxies. The actual galaxies are usually far from such simplified objects. Instead, they contain spiral structure, asymmetries, dust lanes, varying inclination and position angles, etc. So let us take a look at the reproduction of the actual galaxies in the original SDSS images during the creation of the test galaxy sample, which was described in Sect. 2.

Figure 12 shows some examples of the original SDSS images, the model galaxies and the residual images. As expected, spiral structure is still present on the residual images of disc galaxies as well as some asymmetries, which is expected since the model galaxies are axisymmetric. However, no luminosity gradients can be detected, thus the axisymmetric distributions have been recovered correctly.

The upper panel in Fig. 13 shows the distribution of relative differences between the true and modelled luminosities within thin concentric rings as a function of ring radius. For this figure, galaxy sizes are normalised according to their harmonic mean radii a_0. Comparing to the models of test galaxies (Fig. 5) the differences are now slightly larger due to the substructure in actual galaxies.

Lower panel in Fig. 5 shows the distribution of luminosity differences in SDSS standard units (nanomaggies), as measured from the residual images within concentric rings. The differences remain within 1 nanomaggies and do not depend significantly on the distance from the centre of the galaxy.

6. Conclusions

In this paper we have analysed the reliability of 3D structural models created for SDSS galaxies. For the sample extending down to the r-band limiting magnitude 17.77, the accuracy is high for the recovered integral luminosities and colours (0.05 mag), and somewhat lower for the luminosities of individual components (0.2 mag). The bulge-to-disc ratios (B/D) are not very accurate, with typical errors within ±40% of the initial value, but on an average, no sys-

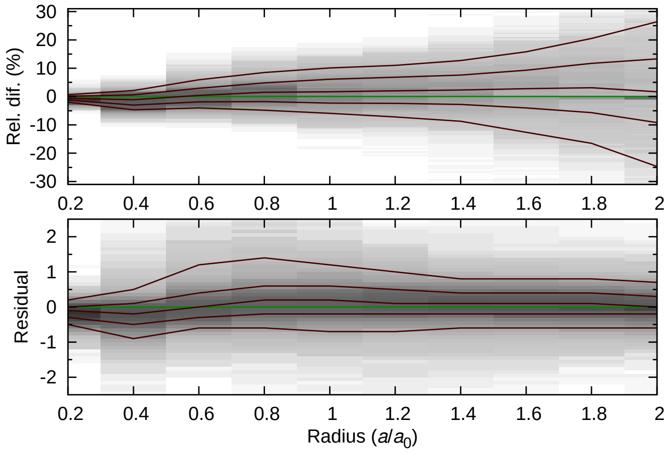

Figure 13: Differences between the observed and modelled luminosities of galaxies, measured inside concentric rings as a function of ring radius. *Upper panel:* luminosity differences divided by the luminosity (per cent). *Lower panel:* residual values in the SDSS standard units, nanomaggies. The ring radii are presented as a fraction of the harmonic mean radius of the given galaxy. *Red solid lines* show the 0.1, 0.25, 0.5, 0.75, and 0.9 quantiles of the distribution.

tematic shift is introduced, thus the method can be used for measuring the statistical bulge and disc fractions in the Universe.

Inclination angle estimates are better for disc-dominated galaxies, with the errors remaining below 5° for galaxies with B/D < 2. Errors of the recovered sizes of the galactic components are less than 10% in most cases. Axial ratios and the parameter N of Einasto's distribution (similar to the Sérsic index) are relatively inaccurate, but can provide statistical estimates for studies of large galactic samples. In general, models of disc components are more accurate than models of bulge components, as can be expected for geometrical reasons.

We can conclude that especially for statistical studies, 3D modelling is worth the extra computation time needed, allowing us to estimate parameters which are not accessible with 2D approaches. The structural parameters, if determined from images only, are not very reliable for any given object.

We have used idealised test galaxies in the presented study. It is natural that the properties of real galaxies are more difficult to determine because of non-symmetries and additional components. An analysis of 3D modelling accuracy of real well-studied nearby galaxies is the topic of a forthcoming paper.

Acknowledgments

We thank E. Saar and J. Pelt for helpful discussion and suggestions. This work was supported by the Estonian Science Foundation grants 7765, 8005, 9428, MJD272 and the Estonian Ministry for Education and Science research projects SF0060067s08. We acknowledge the support by the Centre of Excellence of Dark Matter in (Astro)particle Physics and Cosmology (TK120). All the figures have been made using the gnuplot plotting utility or DS9. Some of the preliminary data analysis have been done with an interactive graphical tool TOPCAT (http://www.starlink.ac.uk/t
We are pleased to thank the SDSS-III Team for the publicly available data releases. Funding for SDSS-III has been provided by the Alfred P. Sloan Foundation, the Participating Institutions, the National Science Foundation, and the U.S. Department of Energy Office of Science. The SDSS-III web site is http://www.sdss3.org/.

References

References

Aihara, H., Allende Prieto, C., An, D., Anderson, S.F., Aubourg, É., Balbinot, E., Beers, T.C., Berlind, A.A., Bickerton, S.J., Bizyaev, D., Blanton, M.R., Bochanski, J.J., Bolton, A.S., Bovy, J., Brandt, W.N., Brinkmann, J., Brown, P.J., Brownstein, J.R., Busca, N.G., Campbell, H., Carr, M.A., Chen, Y., Chiappini, C., Comparat, J., Connolly, N., 2011. ApJS 193, 29.

de Souza, R.E., Gadotti, D.A., dos Anjos, S., 2004. ApJS 153, 411.

Dhar, B.K., Williams, L.L.R., 2010. MNRAS 405, 340.

Einasto, J., 1965. Tartu Astr. Obs. Teated 17.

Einasto, J., Tenjes, P., Barabanov, A.V., Zasov, A.V., 1980. Ap&SS 67, 31.

Lackner, C.N., Gunn, J.E., 2012. MNRAS , 2423.

Peng, C.Y., Ho, L.C., Impey, C.D., Rix, H.W., 2010. AJ 139, 2097.

Sérsic, J.L., 1968. Cordoba, Argentina: Observatorio Astronomico, 1968.

Simard, L., Mendel, J.T., Patton, D.R., Ellison, S.L., McConnachie, A.W., 2011. ApJS 196, 11.

Simard, L., Willmer, C.N.A., Vogt, N.P., Sarajedini, V.L., Phillips, A.C., Weiner, B.J., Koo, D.C., Im, M., Illingworth, G.D., Faber, S.M., 2002. ApJS 142, 1.

Strauss, M.A., Weinberg, D.H., Lupton, R.H., Narayanan, V.K., Annis, J., Bernardi, M., Blanton, M., Burles, S., Connolly, A.J., Dalcanton, J., Doi, M., Eisenstein, D., Frieman, J.A., Fukugita, M., Gunn, J.E., Ivezić, Ž., Kent, S., Kim, R.S.J., Knapp, G.R., Kron, R.G., Munn, J.A., Newberg, H.J., Nichol, R.C., Okamura, S., Quinn, T.R., Richmond, M.W., Schlegel, D.J., Shimasaku, K., SubbaRao, M., Szalay, A.S., Vanden Berk, D., Vogeley, M.S., Yanny, B., Yasuda, N., York, D.G., Zehavi, I., 2002. AJ 124, 1810.

Tamm, A., Tenjes, P., 2006. A&A 449, 67.

Tempel, E., Tago, E. abd Liivamägi, L.J., 2012. A&A 540, A106.

Tempel, E., Tamm, A., Tenjes, P., 2010. A&A 509, A91.

Tempel, E., Tuvikene, T., Tamm, A., Tenjes, P., 2011. A&A 526, A155.

Tenjes, P., Haud, U., Einasto, J., 1994. A&A 286, 753.